Published in final edited form as:
Magn Reson Med. 2017 January ; 77(1): 343–350. doi:10.1002/mrm.26548.

Modeling diffusion of intracellular metabolites in the mouse brain up to very high diffusion-weighting: diffusion in long fibers (almost) accounts for non-monoexponential attenuation

Marco Palombo[1,2], **Clemence Ligneul**[1,2], and **Julien Valette**[1,2]

[1]Commissariat a l'Energie Atomique et aux Energies Alternatives (CEA), Direction de la Recherche Fondamentale (DRF), Institut d'Imagerie Biomedicale (I^2BM), MIRCen, Fontenay-aux-Roses, France

[2]Centre National de la Recherche Scientifique (CNRS), Universite Paris-Sud, Universite Paris-Saclay, UMR 9199, Neurodegenerative Diseases Laboratory, Fontenay-aux-Roses, France

Abstract

Purpose—To investigate how intracellular metabolites diffusion measured *in vivo* up to very high q/b in the mouse brain can be explained in terms of simple geometries.

Methods—10 mice were scanned using our new STE-LASER sequence, at 11.7 T, up to q_{max}=1 μm^{-1} at diffusion time t_d=63.2 ms, corresponding to b_{max}=60 ms/μm^2.

We model cell fibers as randomly oriented cylinders, with radius *a* and intracellular diffusivity D_{intra}^{cyl}, and fit experimental data as a function of q to estimate D_{intra}^{cyl} and *a*.

Results—Randomly oriented cylinders account well for measured attenuation, giving fiber radii and D_{intra}^{cyl} in the expected ranges (0.5-1.5 μm and 0.30-0.45 μm^2/ms, respectively). The only exception is NAA (extracted $a \sim 0$).

We show that is compatible with a small fraction of the NAA pool being confined in highly restricted compartments (with short T_2).

Conclusion—The non-monoexponential signal attenuation of intracellular metabolites in the mouse brain can be described by diffusion in long and thin cylinders, yielding realistic D_{intra} and fiber diameters. However, this simple model may require small "corrections" for NAA, under the form of a small fraction of the NAA signal originating from a highly restricted compartment.

Keywords

metabolites diffusion; diffusion weighted MRS; geometrical model; cell morphology; cell geometry

Corresponding Author: Marco Palombo, Ph.D.; Commissariat à l'Energie Atomique et aux Energies Alternatives (CEA), Direction de la Recherche Fondamentale (DRF), Institut d'Imagerie Biomédicale (I2BM), MIRCen, 8 Route du Panorama, 92260 Fontenay-aux-Roses, France, Tel. 0033 01 46 54 92 96, marco.palombo@cea.fr.

Europe PMC Funders Author Manuscripts

Introduction

Diffusion-weighted NMR spectroscopy (DW-MRS) is a promising tool which offers the unique ability to noninvasively quantify the translational displacement of endogenous molecules, such as brain metabolites *in vivo* (1,2). In contrast to water molecules, which are ubiquitous in biological tissues, most brain metabolites are confined into the intracellular space and hardly cross biological membranes. Their diffusion properties are thus expected to depend mostly on intracellular parameters such as cytosol viscosity, molecular crowding, size and shape of the cellular compartment. In addition, some metabolites have a preferential cellular compartmentation, which makes these molecules useful cell-specific endogenous probes of the intracellular space: N-acetyl-aspartate and glutamate reside essentially in neurons, whereas myo-inositol and choline are glial markers, thought to be preferentially compartmentalized in astrocytes (3).

Changes in endogenous metabolite apparent diffusivity (ADC) have already been detected in pathologies. Alterations in the diffusion of metabolites are observed after global ischemia (4–9), in multiple sclerosis (10), in brain tumor (11–13), in lupus erythematosus (14). Although alterations of intracellular diffusion during brain pathologies are often thought to be associated with cell structural damage; the influence of various parameters (viscosity, molecular crowding, cell size and geometry…) on DW-MRS measurement is still unclear, and the interpretation of experimental data remains complex.

It has been recently shown that the ADC values of these intracellular metabolites in the primate brain and human gray (GM) and white matter (WM) are essentially constant as the diffusion time t_d is increased from a few tens of ms to ~1 sec (15,16). This led us to conclude that the vastest fraction of each metabolite pool is not restricted in small subcellular domains (cell bodies, organelles…) but is instead “freely” diffusing along cell fibers. Going one step further, performing metabolites ADC measurements for the same metabolites at ultra-long t_d (~2 sec.) *in vivo* in mouse and macaque brains and modeling brain cells as long and thin fibers with some finite length and number of successive embranchments, we recently extracted brain cell morphology in very good agreement with histological data (17), thus consolidating the metabolites cell-specific compartmentalization and the view that metabolites are diffusing in fibers.

Above measurements of ADC as a function of t_d were all performed at relatively low b value (~3 ms/μm^2, i.e. weak gradient strength), where diffusion attenuation can be considered as monoexponential. However, it has been shown in other works that, for the same metabolites, diffusion at very high b (i.e. strong gradient strength) exhibits a non-monoexponential behavior in the brain (18–20).

In this work, we investigate how diffusion of these metabolites measured *in vivo* in the healthy mouse brain up to very high q (1 μm^{-1}) at relatively short diffusion time (63.2 ms), corresponding to very high b = 60 ms/μm^2, can be explained by the (admittedly) simplistic view of diffusion in cylinders. We model cell fibers as isotropically oriented cylinders of infinite length and finite diameter, and show this can account very well for measured non-monoexponential attenuation. The only exception is NAA, for which the model extracts fiber

diameter close to 0. We show that is theoretically and experimentally compatible with a small fraction of the NAA pool being confined in highly restricted compartments (with short T_2), e.g. a mitochondrial or myelin pool.

Methods

Data analyzed here are those recently published in (20). Briefly, acquisitions were performed in a large voxel of the mouse brain containing mostly gray matter (~80%), using our new STE-LASER sequence, based on a diffusion-weighted stimulated echo block followed by a LASER localization block, yielding no cross terms between diffusion and selection gradients. 10 mice were scanned at 11.7 T Bruker scanner (g_{max}=752 mT/m) using a cryoprobe, at TE=33.4 ms and t_d=63.2 ms, up to q_{max}=1 μm^{-1} (b_{max}=60 ms/μm^2) (Fig.1a). Individual scan phasing was performed and experimental macromolecule spectrum was included in LCModel's basis-set. Signal attenuation could be reliably quantified (Cramér-Rao lower bound <5% at all b) for NAA, total creatine, choline compounds, myo-inositol, glutamate, and taurine (for further details on the acquisition methods, see (20)).

Unlike biological water, metabolites are mainly intracellular, and membranes are nearly impermeable to metabolites. Cellular processes can be described in first approximation as a collection of long cylinders (Fig.1b) with radius a, and intracellular diffusivity D_{intra}^{cyl}. We assume cylinders randomly oriented to calculate signal attenuation in the narrow pulse approximation. The signal represents the sum of signals from a large number of differently oriented fibers. For any given fiber, the axis makes a variable angle θ with the diffusion gradient, leading to two diffusion regimes: i) restricted diffusion in the plan perpendicular to their axis resulting in an effective gradient strength $g\,sin(\theta)$ and ii) free diffusion in the direction parallel to their axis resulting in an effective gradient strength $g\,cos(\theta)$.

When gradient is separated by an angle θ relative to the axis of the cylinder of radius a, the echo attenuation is given by the following expressions (21,22):

$$E_{cyl}^{a}(g,\delta,t_d)=\left\{\frac{[2J_1\gamma g_\perp \delta a]^2}{(\gamma g_\perp \delta a)^2}+8(\gamma g_\perp \delta a)^2 A_{nm}\right\} e^{-D_{intra}^{cyl}(\gamma g_\parallel \delta)^2 t_d} \quad [1]$$

with

$$A_{nm}=\sum_{n=0}^{\infty}\left\{\frac{1}{1+\delta_{n0}}\left[J_n'\gamma g_\perp \delta a\right]^2 \sum_{m=1}^{\infty}\frac{\alpha_{nm}^2}{(\alpha_{nm}^2-n^2)[\alpha_{nm}^2-(\gamma g_\perp \delta a)^2]^2} e^{-\frac{D_{\text{intra}}^{cyl}\alpha_{nm}^2 t_d}{a^2}}\right\}$$

and $g_\perp = gsin(\theta)$; $g_\parallel = gcos(\theta)$.

In the above equations, J_n is the Bessel function of integer order n and α_{nm} is the mth positive root of the Bessel equation $J'_n = 0$. δ_{n0} is the Kronecker delta symbol and D_{intra}^{cyl} is the free diffusivity, i.e. the diffusivity along the axis of the cylinder (often even called $D_{//}$).

This theoretical attenuation is used to fit experimental data as a function of $q = \gamma g \delta$ to estimate D_{intra}^{cyl} and a by using a nonlinear least-square regression, based on the trust-region-reflective algorithm implemented in the *lsqcurvefit* function of MATLAB (The MathWorks Inc.). Error on estimated parameters was evaluated using a MonteCarlo (MC) approach (N = 2500 draws). For each draw, random noise (whose standard deviation was estimated from the difference between the best fit and the experimental data) was generated and added to the best fit to generate a new dataset, which could be analyzed using the model.

Results

Extracted model parameters using randomly oriented cylinders

Signal attenuation as a function of q for each metabolite is reported in Fig.2, together with best fits, while extracted parameters and corresponding MC estimated errors are reported in Table 1. Results show that randomly oriented cylinders account well for measured attenuation, giving fiber radii consistent with axons, dendrites and astrocytic processes (a ranging from approximately 0.5 to 1.5 μm), and D_{intra}^{cyl} in the expected range for brain metabolites (0.30-0.45 $\mu m^2/ms$). Interestingly, the two "neuronal" metabolites, NAA and glutamate, have the lowest a (0.024 μm and 0.76 μm, respectively), suggesting that neuronal processes are thinner than glial processes. However, this statement should be considered with caution at that stage, because radius extracted for NAA appears very close to zero, which raises some questions about the validity of the modeling for this metabolite. This point will be investigated in deeper details in the Discussion section, together with further discussion about the assumption of isotropic fiber orientation in the investigated volume.

Sensitivity to different fiber diameters and intracellular diffusivity

In order to show the sensitivity of DW-MRS signal to different fiber radii, signal attenuations as a function of q for two representative metabolites (glutamate, supposedly mainly intra-neuronal; and myo-Inositol, supposedly mainly intra-astrocytic) are reported in Fig.3, together with best fits (black curves) and theoretical predictions (from Eq.[1]) for molecular diffusion in randomly oriented cylinders with D_{intra}^{cyl} set to the values reported in Table 1, but different a, varying from 0.2 to 2.4 μm (blue curves, left column); and with a set to the values reported in Table 1, but different D_{intra}^{cyl}, varying from 0.1 to 1.2 $\mu m^2/ms$ (blue curves, right column). According to the theoretical predictions reported in Fig. 3, an absolute percentage difference in signal attenuation greater than 30% is expected for radius changing from 0.2 to 2.4 μm at high q values (Fig. 3 left column, $q>0.5\ \mu m^{-1}$) while the impact remains small at low q; in contrast, for diffusivity changing from 0.1 to 1.2 $\mu m^2/ms$ the same absolute percentage difference is also expected at lower q values (Fig. 3 right column, $q>0.1\ \mu m^{-1}$).

This demonstrates that DW-MRS signal attenuation changes a lot for fiber radii in the reasonable range 0.2-2.4 μm, confirming the high sensitivity of metabolite signal attenuation to fiber size under the current experimental conditions (i.e. considering the diffusion time and q values used). This is because variations of diffusivity values have a strong impact on signal attenuation at all q/b values (i.e. they induce large variations of S/S_0), while variations of radius values obviously have a much stronger impact on signal attenuation at high

weightings, when the remaining signal mostly reflects the restricted diffusion in the plan perpendicular to fiber direction, which strongly depends on the diameter. In other words, while the radius has almost no effect on the initial points of the signal attenuation (e.g. for q<0.3-0.4 μm^{-1}, see Fig. 3), D_{intra}^{cyl} has a strong effect on these initial points, so these initial points can be modeled to provide a reliable estimate of D_{intra}^{cyl} without confounding effect from the radius. Then, at sufficiently high q, varying D_{intra}^{cyl} only results in an offset of the signal attenuation (see on Fig. 3 how all curves are parallel at high q when D_{intra}^{cyl} is varied), but no change in the slope of the curve. On the contrary, the diameter has a stronger effect on the curvature of the signal attenuation at high q, thus carrying the information about the radius without confounding effect from D_{intra}^{cyl}. In the end, although model sensitivity to both parameters is very high, it is possible to disentangle the effect of both parameters depending on the range of q considered, and hence fit both of them reliably.

It is important to underline that here the diffusion of metabolites is investigated. In contrast to water, metabolites diffusion coefficient is much lower (roughly six times lower in physiological conditions), allowing to experimentally probe the finer structures of cells, like branch diameter, which are instead less accessible to water diffusion based NMR techniques at experimentally achievable values of t_d and q (or b): $t_d \geq 20$ ms and $q \leq 0.2$ μm^{-1} (or b≤10 ms/μm^2). In fact, assuming a diffusivity of 2.0 μm^2/ms for water and 0.4 μm^2/ms for metabolites, and t_d=60 ms and a maximum q of 0.2 μm^{-1} (i.e. lower than used in the present study), the absolute percentage difference between the logarithm of the expected diffusion weighted NMR signal from randomly oriented cylinders with a=0.2 μm and a=2.4 μm, computed by using Eq. [1], is ~14% for water and ~26% for metabolites. This suggests that thanks to their slower diffusivity, metabolites' diffusion weighted signal is twice more sensitive to branch diameter than water's. Moreover, for metabolites it is possible to increase even more this sensitivity, pushing the acquisition up to much higher q and b values, while keeping the signal-to-noise ratio relatively high (as shown by spectra in Fig.1a).

Discussion

About the isotropic fiber orientation in the investigated volume

The basic assumption leading to Eq.[1], used to model metabolites diffusion data, is that fibers orientation in the considered voxel is isotropic. This may be true, at least in first approximation, for the metabolites predominantly compartmentalized in GM and astrocytes, but may not be true for those metabolites mainly residing in WM axons. Indeed, the orientation of WM fiber bundles within the investigated voxel is not perfectly isotropic. However, a deeper analysis, including information from DTI metrics, shows that this can be reasonably neglected considering the actual voxel tissue composition: 20% WM and 80% GM (see Supporting Information and Supporting Fig. S1). Although the WM fiber distribution within the voxel is not isotropic, it contributes to the total signal attenuation for a small fraction (i.e. 20%), which leads to estimated a and D_{intra}^{cyl} values only ~4% and ~1% lower than the ones obtained when including the actual angular distribution of fibers in WM (see Supporting Information, Supporting Fig. S2 and Supporting Table S1). We thus found that, although simplistic, the model in Eq.[1] is a very good approximation for the large spectroscopic voxel considered in this study. In fact, the bias on parameters estimation

is lower than the uncertainty on their estimation, according to the Monte Carlo study of fit stability to experimental noise (see Table 1 and 2).

Possible presence of a slowly diffusing NAA pool

Between all the metabolites investigated, NAA represents an exceptional case, because the model extracts a~0. Although a=0 has been used as an assumption to fit NAA diffusion in the past (23–26), in papers where only NAA was reported and analyzed, we think this is not satisfactory, considering that this does not hold for all the other metabolites (including glutamate which is supposed to be, like NAA, predominantly neuronal). Explanations based on finer structural features (e.g. spines, leaflets or varicosities) affecting diffusion of the cytosolic pool also seem unlikely, because they should apply to other metabolites diffusing in the same cells. We should instead primarily seek for a metabolite-specific explanation.

NAA is synthesized in neuronal mitochondria, so it may be significantly present in mitochondria (which represent 5-10% of the cytoplasmic volume), resulting in a second NAA pool, with limited exchange with cytosolic NAA. As mitochondrial matrix is viscous and densely filled with membranes, it is expected that T_2 is very short. Hence, mitochondrial NAA should become invisible at long TE. Consistently, we have measured that, at longer TE (73.4 ms), signal attenuation was slightly but significantly larger for NAA at high q (Fig.4b) than at shorter TE (33.4 ms), while TE had not effect on signal attenuation for the other metabolites (20). When analyzing NAA signal acquired at longer TE with the randomly oriented cylinders model (Fig.4b and Table 2), the model returns a=0.62±0.12 μm (and D_{intra}^{cyl}=0.335±0.021 μm^2/ms), which is now realistic and very close to the radius extracted for glutamate, strongly suggesting that a highly restricted NAA pool has become invisible. Going one step further, these a and D_{intra}^{cyl} values can be injected in a modified model, where a log-normal distribution of spherical compartments (accounting for organelles/ mitochondria size distribution in healthy cells (27,28)) is added to cylinders whose properties were determined at long TE, to fit data at short TE (Fig. 4a-b).

$$E_{tot}(q,t_d) = v_{sph}\frac{\int_0^\infty dr\, r^3 P(r)\, E_{sph}^r(q,t_d)}{\int_0^\infty dr\, r^3 P(r)} + (1-v_{sph})\, E_{cyl}^a(q,t_d) \quad [2]$$

where E_{sph}^r is the echo attenuation for diffusion within a sphere of radius r, in the narrow pulse approximation (21,22):

$$E_{sph}^r(g,\delta,t_d) = \frac{\left[3\, j_1(\gamma g \delta\, r)\right]^2}{(\gamma g \delta\, r)^2} + 6\,(\gamma g \delta\, r)^2 B_{nm}$$

with

$$B_{nm} = \sum_{n=0}^{\infty}\left\{\left[j_n'\,\gamma g\delta\, r\right]^2 \sum_{m=1}^{\infty}\frac{(2n+1)\,\alpha_{nm}^2}{(\alpha_{nm}^2 - n^2 - n)\left[\alpha_{nm}^2 - (\gamma g\delta\, r)^2\right]^2} e^{-D_{intra}^{sph}\alpha_{nm}^2 t_d}\right\}$$

where $j_n(x)$ is the spherical Bessel function of the first kind and α_{nm} is the mth positive root of the Bessel equation $j'_n = 0$.

New free parameters are the diffusivity inside spheres D_{intra}^{sph}, the volume fraction of these spheres v_{sph}, and the mean radius μ and s.d. σ of spheres. Best fit of NAA attenuation at short TE yields (Table 2): v_{sph}=2.0±1.0 %, D_{intra}^{sph}=0.168±0.081 μm^2/ms, μ=0.019±0.010 μm, σ=0.028±0.016 μm. Values of v_{sph} and D_{intra}^{sph} are consistent with the known mitochondrial volume fraction and the higher viscosity in mitochondria. Extracted radii are much smaller than typical mitochondria size, but very consistent with the typical distance between cristae, which must cause most of the restriction inside mitochondria (29).

Arguably the modified model adds some complexity and instability to the model, and requires additional data acquired at longer TE to “delete” the potential short T2 pool. Considering the very small size of the compartments restricting NAA diffusion, estimated by using the data at longer and shorter TE, it is reasonable to simplify Eq.[2], considering the compartments to be very small and the corresponding signal very close to 1 (basically a pool of not-diffusing NAA molecules), thus obtaining:

$$E_{tot}(q,t_d) = v + (1-v)\,E^{a}_{cyl}(q,t_d) \quad [3]$$

where v is now the fraction of not-diffusing NAA. Fitting Eq. [3] to NAA data acquired only at TE=33.4 ms gives: D_{intra}^{cyl}=0.374±0.023 μm^2/ms; a=0.93±0.22 μm and v=8±3 %, which are coherent with the previous results obtained by the modified randomly oriented cylinders model (Table 2) and with the expected fraction of NAA molecules highly restricted in small compartments (e.g. mitochondria).

Note that here we have based our argumentation on a mitochondrial pool, however the argumentation remains valid for any highly restricted pool, such as a potential NAA pool within myelin layers.

Effect of a slowly diffusing NAA pool on long t_d data

Diffusivity values reported in Table 1 are in very good agreement with those recently extracted from ADC measurements performed at very long t_d (and low b) in mouse brain (Table 1 in (17)). However, the only exception is again NAA, for which the estimated D_{intra} here is significantly higher than that reported in (17). This difference can be well explained by considering the effect of a slowly diffusing, highly restricted NAA pool on ADC time dependence at long t_d. Fig. 5 shows the ADC time dependence simulated from a synthetic tissue of 2500 cell-graphs generated according to the new modeling paradigm and the morphometric statistics reported in (17) for NAA, adding a variable small fraction v of not-diffusing NAA. When fitting these long t_d ADCs using the modeling approach described in (17), the effect of a small fraction of slowly diffusing NAA pool is to decrease the value of the estimated D_{intra}, while not affecting the evaluation of the morphometric statistics describing the NAA compartment morphology, demonstrating the robustness of the approach to extract morphometric statistics despite the potential presence of a small immobile metabolite fraction. We found that the true D_{intra} value is underestimated

according to the linear relation: $D_{intra}^{*} = D_{intra} - 0.64\ v$, where D_{intra}^{*} is the estimated D_{intra} from ADC time dependence at long t_d. Using this phenomenological relation to consider the effect of slowly diffusing NAA pool, and the estimated D_{intra}^{*} value reported in (17): 0.306 $\mu m^2/ms$, we get D_{intra} in the range 0.338-0.370 $\mu m^2/ms$, for v in the expected range 5-10%. These values are now in good agreement with the estimated diffusivities using the modified randomly oriented cylinders model (Table 2) and Eq.[3].

Conclusions

The non-monoexponential signal attenuation of intracellular metabolites in the mouse brain can be essentially described by diffusion in long and thin cylinders, yielding realistic D_{intra} and fiber diameters, thus consolidating the view that metabolites diffusion is characteristic of diffusion in long and thin fibers, as previously proposed based on ADC measurements performed at long t_d (and low b) (15–17). However, this simple model seems to require some small “corrections” for NAA at very high b, under the form of a small fraction of the NAA signal originating from a highly restricted (with short T_2) compartment, e.g. a mitochondrial or myelin pool.

The extent of axonal and dendrites damage has been suggested to be a key predictor of outcome in human central nervous system diseases (30,31). It has also been reported that neuronal damage is dependent on axon and dendrites diameter in various neural disorders. For example, for acute and chronic lesions in multiple sclerosis, direct axon counting in post-mortem tissue has suggested that smaller axons might have a greater susceptibility to damage (32). In addition, traumatic brain injury causes significant axonal swelling, and the extent of swelling has been reported to be correlated with survival time (33). Moreover, a significant decrease in dendrites orientation dispersion and density was observed in substantia nigra pars compacta (SNc) and basal ganglia in Parkinson’s disease (34). This decrease is thought to reflect a decrease in the SNc neurite density and reduction in dendritic length and size. We found that these studies all indicate that axon and dendrites diameter is an important metric to evaluate or to predict the progress of different neurological disorders, and hence more precise measurements of such diameters have significant potential in many clinical applications. In fact, although reaching sufficiently high b values on clinical scanner is still very difficult, new techniques are already available to reach b values up to 20 $ms/\mu m^2$, with good SNR for some metabolites (tCho, tCr and NAA) (35), opening the way for promising applications of the modeling proposed here.

Supplementary Material

Refer to Web version on PubMed Central for supplementary material.

Acknowledgments

This work was supported by the European Research Council (Grant 336331). The 11.7-T MRI scanner was funded by a grant from “Investissementd’Avenir–ANR-11-INBS-0011” NeurATRIS: A Translational Research Infrastructure for Biotherapies in Neurosciences.

References

1. Nicolay K, Braun KP, Graaf RA, Dijkhuizen RM, Kruiskamp MJ. Diffusion NMR spectroscopy. NMR in biomedicine. 2001; 14(2):94–111. [PubMed: 11320536]
2. Ronen I, Valette J. Diffusion-weighted magnetic resonance spectroscopy. eMagRes. 2015; 4:733–750.
3. Choi JK, Dedeoglu A, Jenkins BG. Application of MRS to mouse models of neurodegenerative illness. NMR in biomedicine. 2007; 20(3):216–237. [PubMed: 17451183]
4. Wick M, Nagatomo Y, Prielmeier F, Frahm J. Alteration of intracellular metabolite diffusion in rat brain in vivo during ischemia and reperfusion. Stroke. 1995; 26(10):1930–1933. discussion 1934. [PubMed: 7570750]
5. van der Toorn A, Dijkhuizen RM, Tulleken CA, Nicolay K. Diffusion of metabolites in normal and ischemic rat brain measured by localized 1H MRS. Magnetic resonance in medicine : official journal of the Society of Magnetic Resonance in Medicine / Society of Magnetic Resonance in Medicine. 1996; 36(6):914–922.
6. Dijkhuizen RM, de Graaf RA, Tulleken KA, Nicolay K. Changes in the diffusion of water and intracellular metabolites after excitotoxic injury and global ischemia in neonatal rat brain. Journal of cerebral blood flow and metabolism : official journal of the International Society of Cerebral Blood Flow and Metabolism. 1999; 19(3):341–349.
7. Abe O, Okubo T, Hayashi N, Saito N, Iriguchi N, Shirouzu I, Kojima Y, Masumoto T, Ohtomo K, Sasaki Y. Temporal changes of the apparent diffusion coefficients of water and metabolites in rats with hemispheric infarction: experimental study of transhemispheric diaschisis in the contralateral hemisphere at 7 tesla. Journal of cerebral blood flow and metabolism: official journal of the International Society of Cerebral Blood Flow and Metabolism. 2000; 20(4):726–735.
8. Dreher W, Busch E, Leibfritz D. Changes in apparent diffusion coefficients of metabolites in rat brain after middle cerebral artery occlusion measured by proton magnetic resonance spectroscopy. Magnetic resonance in medicine : official journal of the Society of Magnetic Resonance in Medicine / Society of Magnetic Resonance in Medicine. 2001; 45(3):383–389.
9. Zheng DD, Liu ZH, Fang J, Wang XY, Zhang J. The effect of age and cerebral ischemia on diffusion-weighted proton MR spectroscopy of the human brain. AJNR Am J Neuroradiol. 2012; 33(3):563–568. [PubMed: 22081680]
10. Wood ET, Ronen I, Techawiboonwong A, Jones CK, Barker PB, Calabresi P, Harrison D, Reich DS. Investigating axonal damage in multiple sclerosis by diffusion tensor spectroscopy. The Journal of neuroscience : the official journal of the Society for Neuroscience. 2012; 32(19):6665–6669. [PubMed: 22573688]
11. Hakumaki JM, Poptani H, Puumalainen AM, Loimas S, Paljarvi LA, Yla-Herttuala S, Kauppinen RA. Quantitative 1H nuclear magnetic resonance diffusion spectroscopy of BT4C rat glioma during thymidine kinase-mediated gene therapy in vivo: identification of apoptotic response. Cancer Res. 1998; 58(17):3791–3799. [PubMed: 9731486]
12. Harada M, Uno M, Hong F, Hisaoka S, Nishitani H, Matsuda T. Diffusion-weighted in vivo localized proton MR spectroscopy of human cerebral ischemia and tumor. NMR in biomedicine. 2002; 15(1):69–74. [PubMed: 11840555]
13. Valette J, Giraudeau C, Marchadour C, Djemai B, Geffroy F, Ghaly MA, Le Bihan D, Hantraye P, Lebon V, Lethimonnier F. A new sequence for single-shot diffusion-weighted NMR spectroscopy by the trace of the diffusion tensor. Magnetic resonance in medicine : official journal of the Society of Magnetic Resonance in Medicine / Society of Magnetic Resonance in Medicine. 2012
14. Ercan E, Magro-Checa C, Valabregue R, Branzoli F, Wood ET, Steup-Beekman GM, Webb AG, Huizinga TW, van Buchem MA, Ronen I. Glial and axonal changes in systemic lupus erythematosus measured with diffusion of intracellular metabolites. Brain : a journal of neurology. 2016; 139(Pt 5):1447–1457. [PubMed: 26969685]
15. Najac C, Marchadour C, Guillermier M, Houitte D, Slavov V, Brouillet E, Hantraye P, Lebon V, Valette J. Intracellular metabolites in the primate brain are primarily localized in long fibers rather than in cell bodies, as shown by diffusion-weighted magnetic resonance spectroscopy. NeuroImage. 2014; 90:374–380. [PubMed: 24382523]

16. Najac C, Branzoli F, Ronen I, Valette J. Brain intracellular metabolites are freely diffusing along cell fibers in grey and white matter, as measured by diffusion-weighted MR spectroscopy in the human brain at 7 T. Brain structure & function. 2016; 221(3):1245–1254. [PubMed: 25520054]
17. Palombo M, Ligneul C, Najac C, Le Douce J, Flament J, Escartin C, Hantraye P, Brouillet E, Bonvento G, Valette J. New paradigm to assess brain cell morphology by diffusion-weighted MR spectroscopy in vivo. Proceedings of the National Academy of Sciences of the United States of America. 2016; 113(24):6671–6676. [PubMed: 27226303]
18. Pfeuffer J, Tkac I, Gruetter R. Extracellular-intracellular distribution of glucose and lactate in the rat brain assessed noninvasively by diffusion-weighted 1H nuclear magnetic resonance spectroscopy in vivo. Journal of cerebral blood flow and metabolism : official journal of the International Society of Cerebral Blood Flow and Metabolism. 2000; 20(4):736–746.
19. Assaf Y, Cohen Y. In vivo and in vitro bi-exponential diffusion of N-acetyl aspartate (NAA) in rat brain: a potential structural probe? NMR in biomedicine. 1998; 11(2):67–74. [PubMed: 9608590]
20. Ligneul C, Palombo M, Valette J. Metabolite diffusion up to very high b in the mouse brain in vivo: Revisiting the potential correlation between relaxation and diffusion properties. Magnetic resonance in medicine : official journal of the Society of Magnetic Resonance in Medicine / Society of Magnetic Resonance in Medicine. 2016
21. Neuman CH. Spin-Echo of Spins Diffusing in a Bounded Medium. Journal of Chemical Physics. 1974; 60(11):4508–4511.
22. Linse P, Soderman O. The Validity of the Short-Gradient-Pulse Approximation in Nmr-Studies of Restricted Diffusion - Simulations of Molecules Diffusing between Planes, in Cylinders and Spheres. J Magn Reson Ser A. 1995; 116(1):77–86.
23. Assaf Y, Cohen Y. Structural information in neuronal tissue as revealed by q-space diffusion NMR spectroscopy of metabolites in bovine optic nerve. NMR in biomedicine. 1999; 12(6):335–344. [PubMed: 10516615]
24. Assaf Y, Cohen Y. Assignment of the water slow-diffusing component in the central nervous system using q-space diffusion MRS: implications for fiber tract imaging. Magnetic resonance in medicine : official journal of the Society of Magnetic Resonance in Medicine / Society of Magnetic Resonance in Medicine. 2000; 43(2):191–199.
25. Cohen Y, Assaf Y. High b-value q-space analyzed diffusion-weighted MRS and MRI in neuronal tissues - a technical review. NMR in biomedicine. 2002; 15(7-8):516–542. [PubMed: 12489099]
26. Kroenke CD, Ackerman JJ, Yablonskiy DA. On the nature of the NAA diffusion attenuated MR signal in the central nervous system. Magnetic resonance in medicine : official journal of the Society of Magnetic Resonance in Medicine / Society of Magnetic Resonance in Medicine. 2004; 52(5):1052–1059.
27. van Tienen FH, Lindsey PJ, van der Kallen CJ, Smeets HJ. Prolonged Nrf1 Overexpression Triggers Adipocyte Inflammation and Insulin Resistance. J Cell Biochem. 2010; 111(6):1575–1585. [PubMed: 21053274]
28. Picard M, Gentil BJ, McManus MJ, White K, St Louis K, Gartside SE, Wallace DC, Turnbull DM. Acute exercise remodels mitochondrial membrane interactions in mouse skeletal muscle. J Appl Physiol. 2013; 115(10):1562–1571. [PubMed: 23970537]
29. Dieteren CE, Gielen SC, Nijtmans LG, Smeitink JA, Swarts HG, Brock R, Willems PH, Koopman WJ. Solute diffusion is hindered in the mitochondrial matrix. Proceedings of the National Academy of Sciences of the United States of America. 2011; 108(21):8657–8662. [PubMed: 21555543]
30. Debanne D, Campanac E, Bialowas A, Carlier E, Alcaraz G. Axon physiology. Physiological reviews. 2011; 91(2):555–602. [PubMed: 21527732]
31. Medana IM, Esiri MM. Axonal damage: a key predictor of outcome in human CNS diseases. Brain : a journal of neurology. 2003; 126:515–530. [PubMed: 12566274]
32. Ganter P, Prince C, Esiri MM. Spinal cord axonal loss in multiple sclerosis: a post-mortem study. Neuropath Appl Neuro. 1999; 25(6):459–467.
33. Wilkinson AE, Bridges LR, Sivaloganathan S. Correlation of survival time with size of axonal swellings in diffuse axonal injury. Acta Neuropathol. 1999; 98(2):197–202. [PubMed: 10442560]

34. Kamagata K, Hatano T, Aoki S. What is NODDI and what is its role in Parkinson's assessment? Expert Rev Neurother. 2016; 16(3):241–243. [PubMed: 26777076]

35. Ingo C, Brink WM, Webb A, Ronen I. Utilizing the improved receive sensitivity from high permittivity materials for SNR-challenged applications of ultrahigh b-factor diffusion-weighted spectroscopy at 7 Tesla. Proc Intl Soc Mag Reson Med. 2016; 24:743.

Europe PMC Funders Author Manuscripts

Europe PMC Funders Author Manuscripts

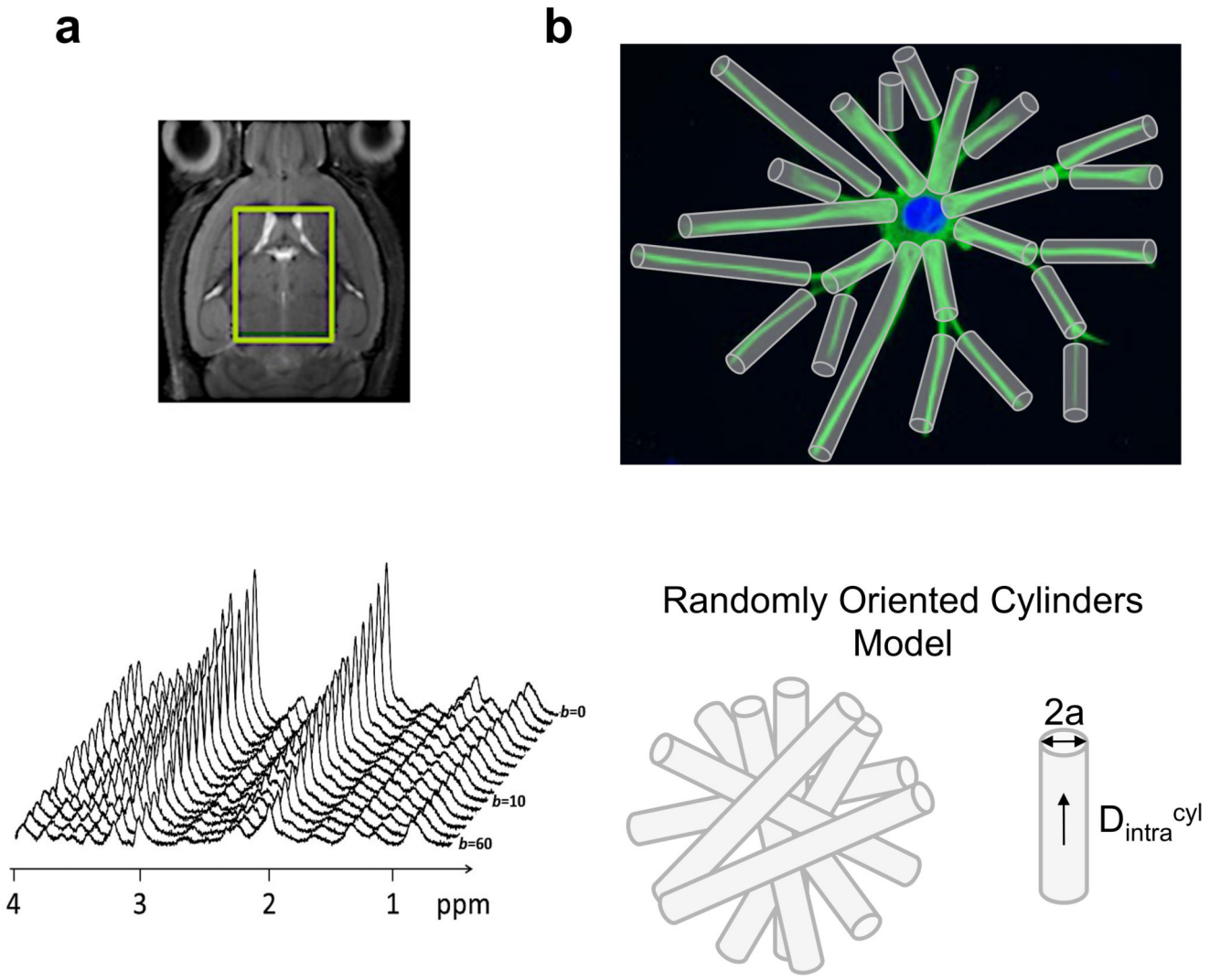

Figure 1.

(a) Diffusion-weighted spectra obtained with the STE-LASER sequence described in *Methods*, at different b-values, during a single experiments. The selected voxel in the mouse brain is shown as green box. (b) Schematic description of the randomly oriented cylinders model used to fit experimental data.

Europe PMC Funders Author Manuscripts

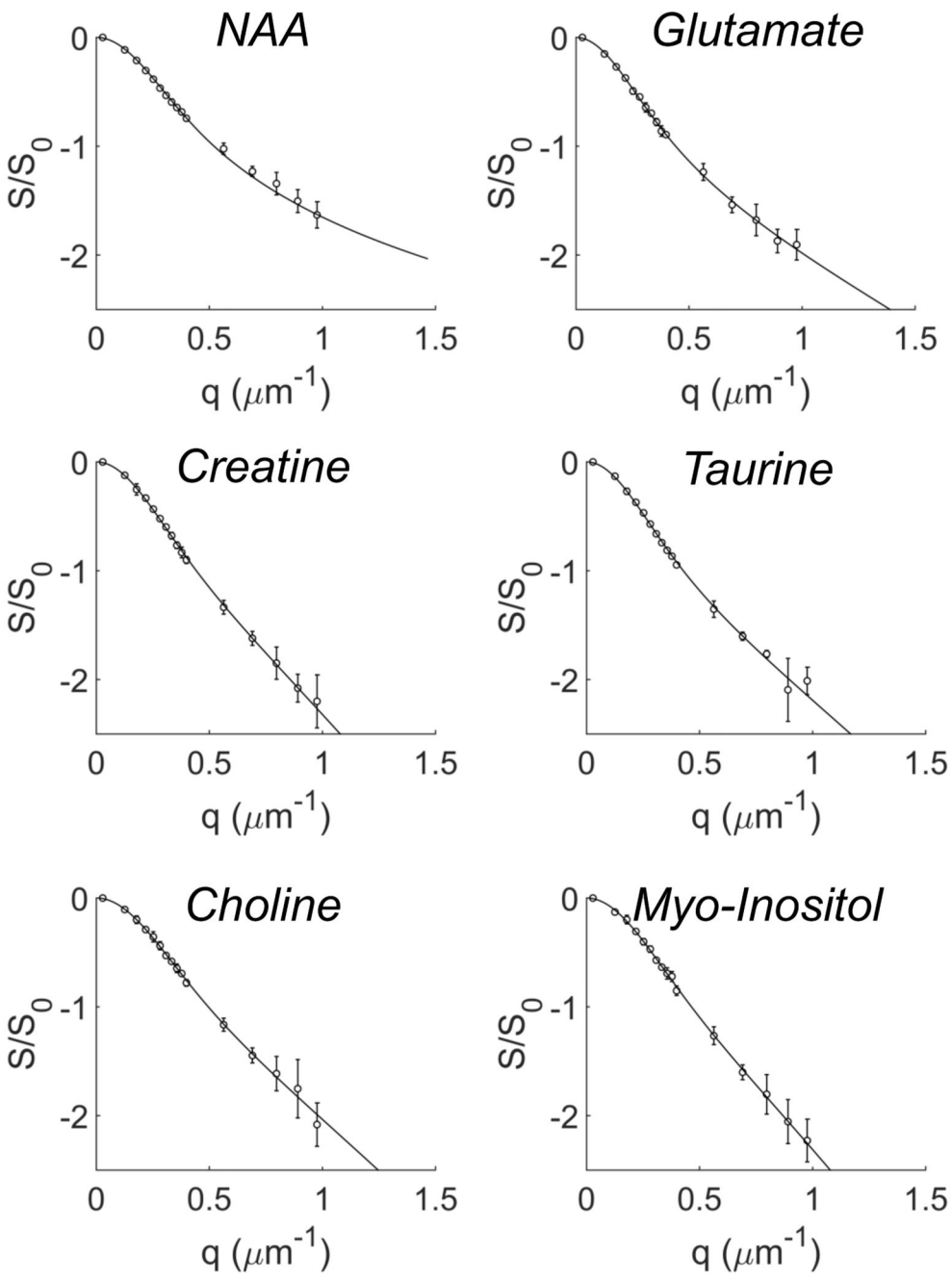

Figure 2.
DW signal attenuation (points) and corresponding fitted curves (lines) as a function of q for all the investigated metabolites. Error bars stand for s.d. of the mean.

Europe PMC Funders Author Manuscripts

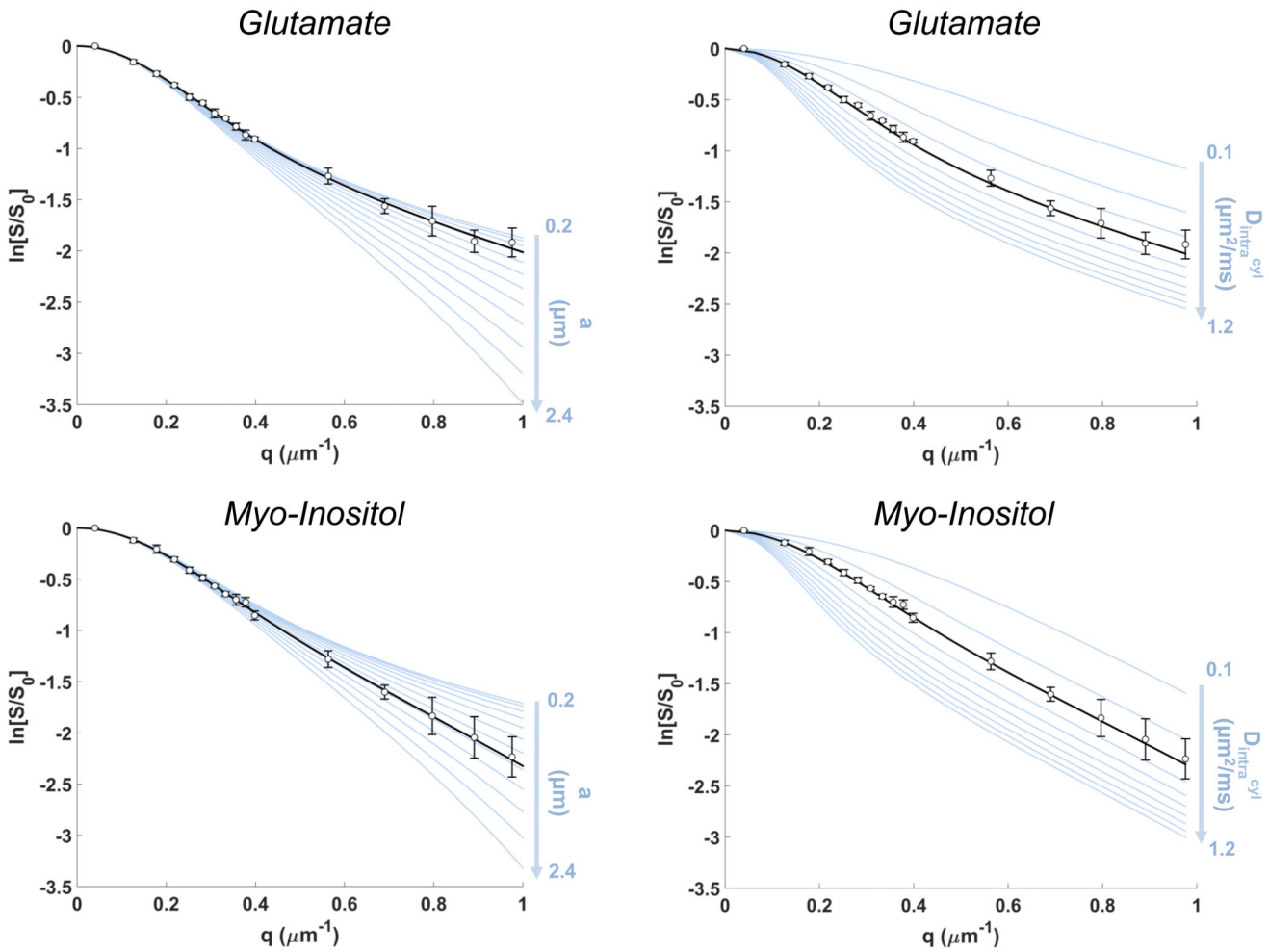

Figure 3.

DW signal attenuation (points) and corresponding fitted curves (black lines) as a function of q for two representative metabolites. Error bars stand for s.d. of the mean and theoretical predictions (from Eq.[1]) for molecular diffusion in random cylinders with D_{intra}^{cyl} set to the values in Table 1, but different *a*, varying from 0.2 to 2.4 μm, are reported as blue curves on the left column. Theoretical predictions (from Eq.[1]) for molecular diffusion in random cylinders with *a* set to the values in Table 1, but different D_{intra}^{cyl}, varying from 0.1 to 1.2 μm^2/ms, are instead reported as blue curves on the right column.

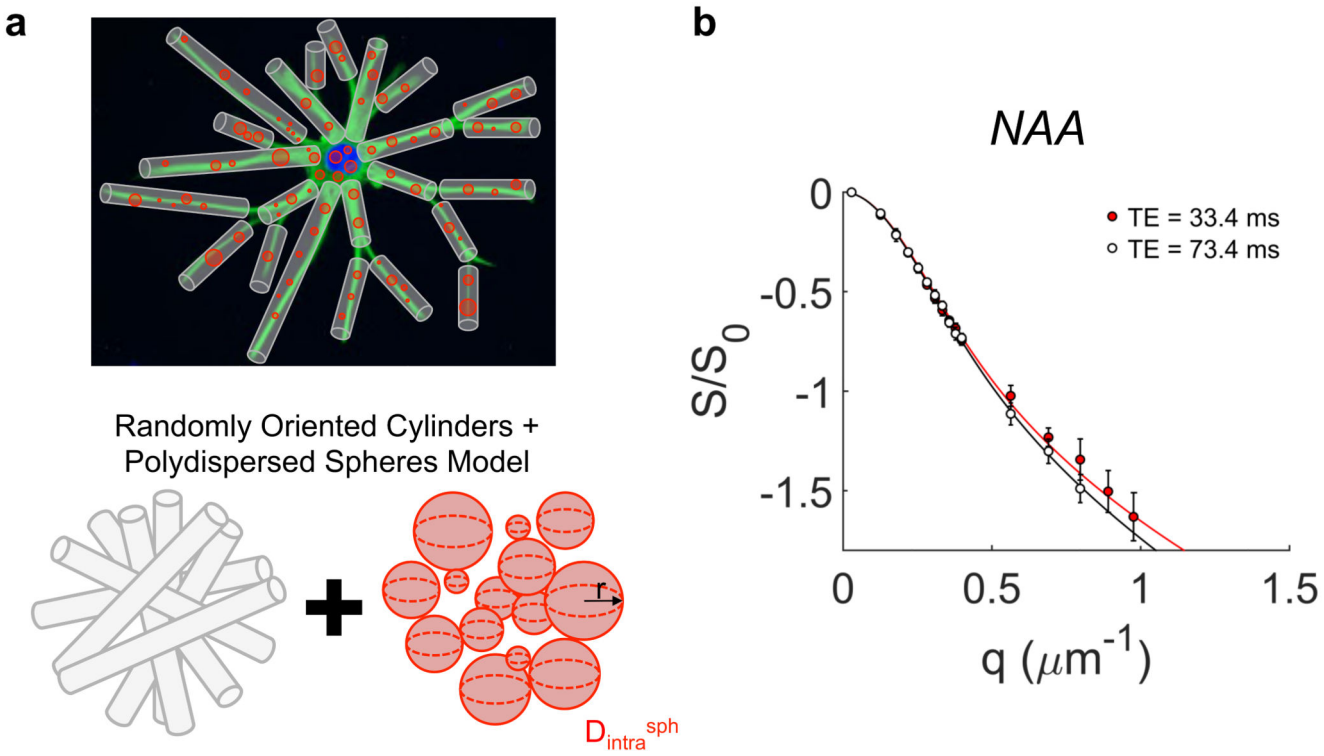

Figure 4.

(a) Schematic description of the modified randomly oriented cylinders model. (b) q dependence of the NAA DW signal attenuation (points) and corresponding fitted curves (randomly oriented cylinders model, black line; modified randomly oriented cylinders model, red line) at short (red) and long (black) TE. Error bars stand for s.d. of the mean.

Europe PMC Funders Author Manuscripts

Europe PMC Funders Author Manuscripts

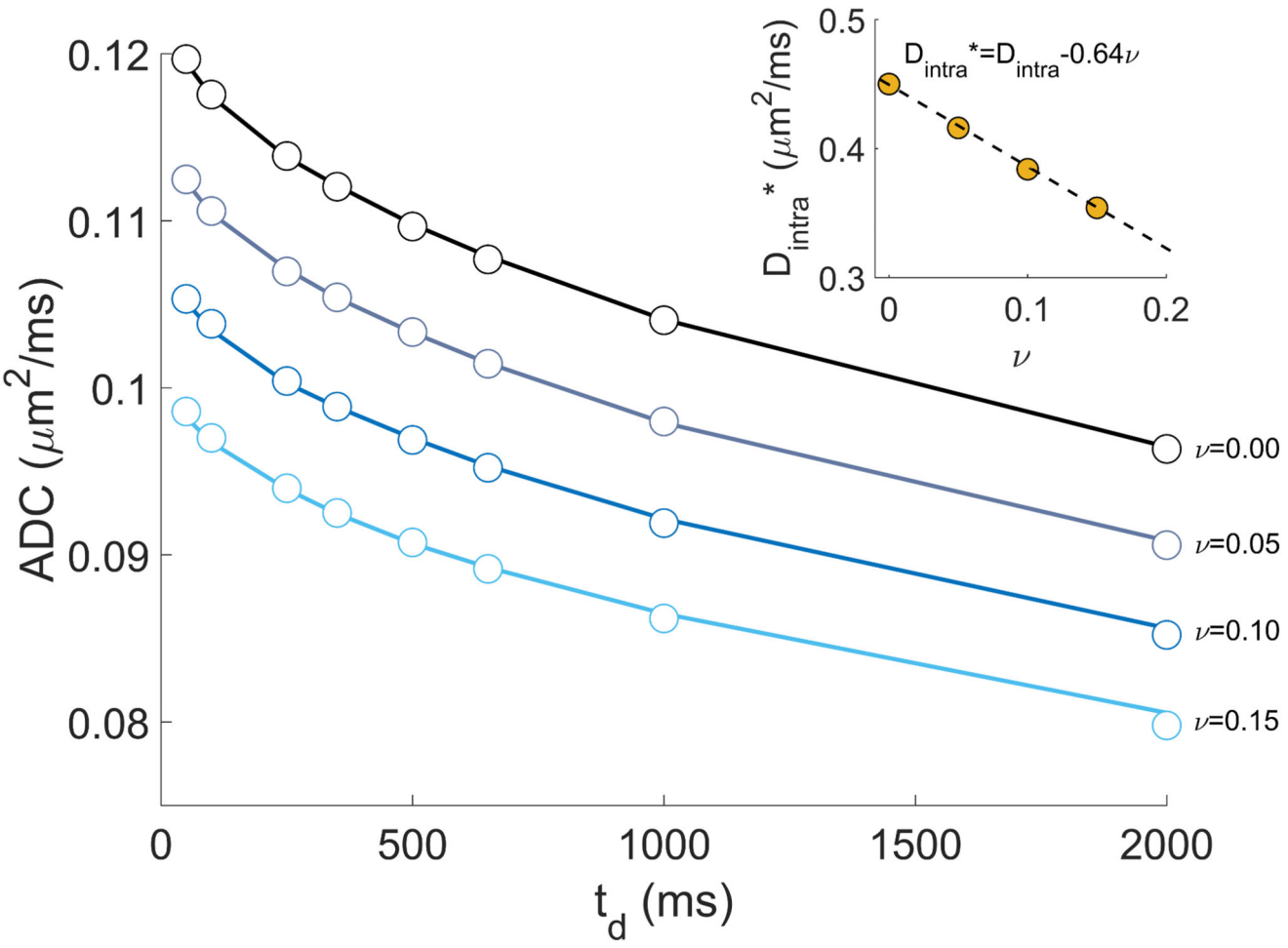

Figure 5.

Data points represent the simulated ADC time dependence for a synthetic tissue comprised of 2500 cell-graphs mirroring the morphometric statistics for NAA, as extracted in Table1 in (17): N_{branch} = 4; $L_{segment}$ = 60 μm; $SD_{Nbranch}$ = 2; $SD_{Lsegment}$= 5 μm, at different v values. Curves are the best fits using the simulation-fitting pipeline described in (17). Fitting pipeline extracted the same morphometric statistics but different D_{intra}* values from the true imposed one: D_{intra} = 0.45 μm^2/ms.These values are reported in the inset as a function of v, with the linear relation: D_{intra}* = D_{intra} + A v fitted to the data, giving A = -0.64 μm^2/ms.

Europe PMC Funders Author Manuscripts

Table 1

Estimated model parameters from the fit of the randomly oriented cylinders model to experimental data of each metabolite, obtained with the Monte Carlo analysis. D_{intra}^{cyl}= intracellular diffusivity and a = cylinders radius (mean ± s.d., 2500 Monte Carlo draws).

Metabolite	D_{intra}^{cyl} ($\mu m^2/ms$)	a (μm)
NAA	0.332 ± 0.011	0.024 ± 0.083
Glutamate	0.439 ± 0.018	0.76 ± 0.16
Creatine	0.369 ± 0.016	1.429 ± 0.087
Taurine	0.416 ± 0.018	1.15 ± 0.10
Choline	0.311 ± 0.015	1.260 ± 0.095
Myo-Inositol	0.328 ± 0.015	1.554 ± 0.080

Table 2

Estimated model parameters from the fit of the randomly oriented cylinders model to experimental data of NAA at TE=73.4 ms and the modified randomly oriented cylinders model to experimental data of NAA at TE=33.4 ms (mean ± s.d., 2500 Monte Carlo draws).

Metabolite	D_{intra}^{cyl} *(μm²/ms)*		*a (μm)*	
NAA (TE=73.4 ms)	0.335 ± 0.021		0.62 ± 0.12	
Metabolite	D_{intra}^{sph} ***(μm²/ms)***	***μ (μm)***	***σ (μm)***	v_{sph} ***(%)***
NAA (TE=33.4 ms)	0.168 ± 0.081	0.019 ± 0.010	0.028 ± 0.016	2.0 ± 1.0